Fermi National Accelerator Laboratory

FERMILAB-FN-598

Study of the Process $H(800) \rightarrow Z_1 Z_2$, $Z_1 \rightarrow q\bar{q}$, $Z_2 \rightarrow \tau_1 \tau_2$, $\tau_{1,2} \rightarrow \rho\nu$ for the SDC Calorimeter

W. Wu, A. Beretvas, D. Green and J. Marraffino

Fermi National Accelerator Laboratory, Batavia, Illinois 60510

November 1992

Operated by Universities Research Association Inc. under Contract No. DE-AC02-76CHO3000 with the United States Department of Energy

Disclaimer

Study of the Process H(800) $\rightarrow Z_1 Z_2$,

$Z_1 \rightarrow q\bar{q}$, $Z_2 \rightarrow \tau_1\tau_2$, $\tau_{1,2} \rightarrow \rho\nu$ for the SDC Calorimeter

W. Wu, A. Beretvas, D. Green, and J. Marraffino

Fermi National Accelerator Laboratory, Batavia, Illinois, 60510.

Introduction

The importance of the forward detectors ($3.0 < | \eta | < 6.0$) in hadron collider detectors is not often stressed. In this note we show that the missing energy ($\not\!\!E_T$) resolution for a particular process is considerably improved by the addition of forward detectors. The process we have chosen to investigate is:

$$pp \rightarrow \text{Higgs}(800\,\text{GeV}) \rightarrow Z^0\,Z^0 \rightarrow (q\bar{q})(\tau^+,\tau^-) \rightarrow (q\bar{q})(\rho^+\nu_\tau, \rho^-\overline{\nu}_\tau) \rightarrow (\text{jet}_1\text{jet}_2)(\pi^+\pi^0\nu_\tau, \pi^-\pi^0\overline{\nu}_\tau). \quad (1)$$

The final state that we detect consists of 2 jets, 2 charged pions, 4 gammas, and missing E_T ($\not\!\!E_T$) due to the two neutrinos. This decay mode of the Z puts stringent requirements on the EM calorimeter segmentation[1], because one needs to reconstruct the π^0 mass. Thus, designers of the SDC shower maximum (SM) detector might consider efficient detection of this process to be a design requirement.

The search for the Standard Model Higgs divides into three mass regions (low, intermediate, and high). The high mass region is from $180 < M_{Higgs} < 800$ GeV. The primary detectable decay mode of the Higgs in the heavy mass region is through the mode Z^0Z^0. In turn, the most easily detected mode is when both Z^0 decay into lepton pairs. The cross section is small, see Fig. 1 ($\sim$

4 pb), and when this is combined with the small branching ratio into lepton pairs (0.0011) the number of events in a SSC year is small. The small number of events at the higher end of the mass region is made even more difficult by the large width of the Higgs (Γ = 1.4, 30, 269 GeV for Higgs of mass 200, 400 and 800 GeV). This problem has been investigated in the SDC Technical Design Report [2], and the results are given in Fig. 2. When geometric acceptance and detection efficiency are included the number of events is approximately 12/SSC year for a Higgs mass of 800 GeV.

The mode studied in this paper has about the same branching ratio as the standard lepton mode. Our purpose is to explore which properties of the detector are needed to see the signal. These properties include the angular range of the detector (η region) and the granularity of the shower maximum (SM) detector. Other features which were studied so as to assess sensitivity of the process to them are hermiticity (cracks), noise and threshold, granularity of EM and HAD cells, e/h, and number of overlapped minimum bias events. We have not considered the question of separating the signal from the background. However, we have studied the complete event including background neutrinos from the heavy quark jets.

Generation of events

We use ISAJET version 6.43 to generate events of the type shown in Eq. 1. We have used the program SSCSIM [3],[4],[5] to produce histograms and LEGO plots. The signature for these events will be a "boosted" Z. This high P_T Z will then appear as either two jets from q and $\bar{q}$, or as high P_T π^0 and $\pi^\pm$ forming 2 low mass ρ clusters along with a large $\not{E}_T$ from the two neutrinos. The reconstruction of the transverse mass for the Z^0 proceeds in steps. We first find 2 gammas and reconstruct a π^0. Then we find the other 2 high P_T gammas and again reconstruct a π^0. Next one combines the π^0 with a high P_T π^+ to form a ρ^+. Similarily the other π^0 is matched with a π^- to form a ρ^-. Clearly, in order to reconstruct this decay mode the 2 photons must be resolved in

the SM strip detector. The gamma pair invariant mass must be consistent with a π^0. In order to identify the boosted Z, the transverse mass must be reconstructed.

We define a vector $\vec{P}$ to be the sum:

$$\vec{P}(\rho) = \vec{P}(\rho^+) + \vec{P}(\rho^-). \tag{2}$$

This vector represents the charged and neutral high P_T particles in the event. The square of the transverse mass of the Z^0 is then:

$$M_T^2 = M_T^2(\rho) + 2(E_T(\rho)E_T(\nu) - \vec{P}_T(\rho) \cdot \vec{P}_T(\nu)). \tag{3}$$

The transverse neutrino energy is determined in the standard way by summing the energy in the LEGO plot:

$$E_T(\nu) \equiv \not{E}_T = -\sum_{i=1}^{n} E_T^i \hat{n}_i \tag{4}$$

where $\hat{n}_i$ is a unit vector perpendicular to the beam axis and pointing to center of the ith calorimeter tower. The transverse Z^0 mass distribution as generated by ISAJET is shown in Fig. 3.

Kinematics

In this section we indicate some of the kinematic features of the decay. In Fig. 4 we show the P_T, η, and rapidity (y) distribution of the Higgs. The dip in the center of the η distribution occurs because of the heavy mass of the Higgs. Figure 5 shows the P_T and η distributions for the Z^0. The P_T's for the τ, ρ, ν, π, and γ are given in Fig. 6. As we continue down the decay chain the expected reduction in P_T is observed. When the Higgs mass is heavy, the produced Z^0's have a large Lorentz boost, and the decay products (τ's) will frequently be close to each other (see Fig. 7).

Fig. 8a gives the angular separation of the two gammas from each other. The angular separation as a function of η is given in Fig. 8b. The average opening angle between the two gammas is 14

mrad and the radial distance to the barrel shower maximum detector is about 2.1 m. This means that SM strip widths of roughly 2.9 cm or less, on the scale of the Molière radius (1.23 cm in Pb), are required to separate the 2 photons. Note that the SDC design has SM strips of size 1.25 cm which is clearly near to the appropriate size.

π^0 Reconstruction

We calculate the mass of the π^0 using the two photons. If smearing is assumed, then we smear the vertex of the π^0 (Δ r = 0.25 cm, $\Delta\ \phi$ = 0.001 rad for the central region, Δ z = 0.25 cm, $\Delta\ \phi$ = 0.001 rad elsewhere). Next we find the direction of both of the γ's. We then take the average of the gamma positions as the direction of the π^0. Then we determine the energy of the π^0. The π^0 energy is obtained by using all the energy in a cone of radius R = $\sqrt{(\Delta\eta)^2 + (\Delta\phi)^2}$ = 0.1 in η -ϕ space. This cone is taken to be centered on the average position given by the shower maximum detector. We must use a single cone because of the overlapping energy distributions of the two gammas. If the cone size is too small, not all the energy from both gammas will be included. Clearly, if the cone size is too large there will be additional energy from underlying and overlapping min-bias events. We have determined the optimum cone size by looking at the transverse Z^0 mass distribution. In Fig. 9a we show the π^0 mass using the normal cell size of the EM calorimeter, and in Fig. 9b we show the π^0 mass using the cell size of the shower maximum detector ($\Delta\eta = \Delta\phi = 0.00625$). It is clear that one can not determine the existence of the π^0 without the shower-max detector.

Rho Reconstruction

We do not consider problems related to tracking and take the charged pion track information directly from ISAJET. The mass of the ρ is determined from the momentum of the charged π and the π^0 (the mass cut of 100 MeV to 180 MeV is shown in Fig 9a and b). In Fig. 10a we show the mass of the ρ when we use a cell size corresponding to the of the EM calorimeter ($\Delta\eta = \Delta\phi$

$= 0.05$). In Fig. 10b the ρ mass reconstructed using the cell size of the shower maximum detector ($\Delta\eta = \Delta\phi = 0.00625$) is shown. Note that ISAJET generates a ρ of zero intrinsic width. The ρ peak seen in Fig. 10a is badly degraded without the SM detector. Obviously, the reconstruction algorithm needs to avail itself of the fine granularity afforded by the SM detector.

Missing E_T

The principal source of $\not\!\!E_T$ in these events is the energy from the two neutrinos (ν_τ and $\overline{\nu}_\tau$). Other sources, primarily from jets, are muons and other neutrinos. We correct for the energy taken off by muons by obtaining their momentum from ISAJET and adding it to the hadronic energy in the calorimeter. The neutrinos from the τ decays each contribute of the order of 60 GeV per event, which accounts for 80% of the $\not\!\!E_T$. In Fig. 11 we show three $\not\!\!E_T$ distributions, the first is from ISAJET, the second is for a detector that extends out to $\eta = 5$ which has all options off (see section on real detectors), and the third figure is for the same detector but with all options on.

In order to quantify how well the $\not\!\!E_T$ is measured we define the variable S_{xy} :

$$S_{xy} = \sqrt{(\not\!\!E_x - E_x(\nu))^2 + (\not\!\!E_y - E_y(\nu))^2} \tag{5}$$

The distribution of S_{xy} is given in Fig. 12a. We fit this distribution using a Gaussian and characterize the resolution of the $\not\!\!E_T$ by the sigma of the Gaussian (S_{MET}). Another way of seeing the $\not\!\!E_T$ resolution is from a scatter plot (Fig. 12b) of the measured $\not\!\!E_T$ versus that obtained from ISAJET.

Z^0 Transverse Mass

Given the missing E_T, we can now reconstruct the Z^0 transverse mass (using Eq. 3). The result is shown in Fig. 13 for the case of an ideal detector (all options off) with an EM cell size $\Delta\eta = \Delta\phi = 0.01$. We notice that this distribution is much more Gaussian than that given in Fig. 3. If we fit to a Gaussian, the resulting mean is 75 GeV with a width of 15.7 GeV.

Method of Comparison

In order to compare the resolution under different conditions, we take the ratio of the reconstructed distribution to the one generated by ISAJET. The advantage of the ratio method is that it is quite stable, has a distribution that is almost Gaussian, and is independent of input widths. We use as a figure of merit the sigma based on a Gaussian fit in a region that contains 75% of the events and is centered on the peak. Figure 14 shows the distribution of the transverse Z^0 mass ratio for an ideal detector (all effects turned off) that has EM cell size $\Delta\eta = \Delta\phi = 0.01$ and which extends to $\eta = 5$. Figure 14 is based on the statistics of 1000 events. The sigma is 10.9 ± 0.4 %.

Real Detectors

SSCSIM allows many properties of real detector to be simulated and/or turned off. The "all turned on" option refers to the following conditions; a) uniform solenoidal magnetic field of 1.8 T, b) longitudinal and transverse shower profiles for both photons and hadrons[6], c) energy smearing (see Table 1) $dE = a\sqrt{E} \oplus bE$, d) decay vertex smearing, e) cracks which cover 4.4% of the area (we refer to this as a 2 cm crack), f) noise for each cell is chosen from a Gaussian distribution with a sigma of 200 MeV, g) threshold cut on each cell of 100 MeV energy and h) nonuniformity of photon/hadron response of $(e/h = 1.25)$[7]. In Fig. 15 we show S_{MET} of the detector for an ideal detector (a) and for a real detector (b). In both cases we have used a detector that has coverage out to $\eta = 5$, and "normal" cell size ($\Delta\eta = \Delta\phi = 0.05$ for EM and $\Delta\eta = \Delta\phi = 0.10$ for HAD). We see that the sigma increases from 21.5 GeV to 33.2 GeV. The corresponding ratio plots for the Z^0 transverse mass are given in Fig. 16a and Fig. 16b. The increase in sigma for the ratio is from 11.8% to 14.2%. Unfolding in quadrature, the standard detector then contributes 25.3 GeV to the missing energy resolution.

We now turn to the elements of the detector dependent contribution. Note that the total

detector contribution to the missing energy is comparable to the "intrinsic" contribution.

η Coverage

Table 2 gives results for both a complete detector (η coverage to 5.) and one that extends out to $\eta = 3$. A "perfect" detector for cell size refers to one that has $\Delta\eta = \Delta\phi = 0.01$ for the EM calorimeter and $\Delta\eta = \Delta\phi = 0.02$ for the Hadron calorimeter. We see, as expected, that the best resolution is obtained with a complete detector and "perfect" cell size and all options off. We note that the small cell size helps only when noise and threshold effects are turned off. We see that for "all effects turned on" there is a considerable improvement in resolution between the complete detector and the one that extends out to $\eta = 3$ (14.2% versus 21.4%). The transverse Z^0 mass resolution is degraded by a factor of 50% by using only the detector that extends out to $\eta = 3$.

Cell Size

In Table 2 we consider two possible cell sizes ("perfect" and "normal"). Although with all effects turned off the $\not\!\!E_T$ resolution is much better for the perfect detector, the real detector performance is better with a normal cell size than with the very small cell size. The reason is that the noise and threshold are assumed to be per cell and thus make a much larger contribution with many more small cells. As indicated in Table 2, the normal cell size is good for the $\not\!\!E_T$ resolution. It is not, however, good for measuring the π^0 mass as noted above.

Cracks

The barrel calorimeter is made up of 32 modules placed at a radius of about 2.3 m. The separation of the modules is designed to be at worst 2 cm. This maximum separation results in 4.4% of the energy being lost in the cracks on average. Table 3 shows that if all options are off there is a large difference between a detector that has a no cracks as compared to one that has a 4 cm crack. For a detector with perfect cell size, the $\not\!\!E_T$ resolution changes from 14.5 GeV to 39.6 GeV,

and the corresponding Z^0 transverse mass resolution ratio changes from 10.9% to 16.3%. However, when we consider a normal detector with everything turned on, the $\not{E}_T$ resolution changes from 30.8 GeV to 40.8 GeV (a factor of 32%), and the corresponding Z^0 transverse mass resolution changes from 14.2% to 18.4% (a factor of 30%). Thus a detector with a "large" crack (4 cm), compared to the detector we plan to build (< 2 cm), still does not make the major contribution to the $\not{E}_T$ resolution.

Minimum Bias Events

We next consider the performance of the detector at a luminosity of $10^{34}/(\text{cm}^2\text{sec})$. The results are given in Table 4. At this higher luminosity the transverse Z^0 mass resolution will be degraded by a factor of 23% and the $\not{E}_T$ resolution by a factor of 48%.

Noise and Threshold

For a normal cell size detector the noise and threshold effects make no difference in the $\not{E}_T$ resolution. The relevant numbers are given in Table 5. It is interesting to observe that when noise and threshold are turned on the performance of the detector with standard cell size is not altered. There is a large change in the $\not{E}_T$ resolution (33.1 GeV to 41.8 GeV) for a detector with very small cell size.

Nonuniforimity of photon/hadron response

In Table 6. we show the performance of a detector with all options off and photon to hadron response set equal to 1.25. We see that for the normal cell size the performance is not changed. Hence the nonuniformity of photon/hadron response of our detector is not a consideration of the performance with regard to $\not{E}_T$ resolution.

Conclusions

This study shows that complete η coverage out to $\eta = 5$ is necessary for good $\not{E}_T$ resolution for

the process considered. In particular full coverage ($| \eta | < 5$) yields $S_{xy} = 33$ GeV and coverage out to ($| \eta | < 3$) yields a resolution that is 52 GeV. We have also given quantitative estimates of how both the $\not{E}_T$ resolution and the transverse Z^0 mass resolution are degraded by cracks, high luminosity, and noise and threshold effects. Finally, for this particular process the Shower Maximum detector is needed to reconstruct the π^0.

References

[1] The ALEPH Collaboration,"Measurement of the Polarization of τ Leptons Produced in Z Decays", CERN-PPE/91-94 (June 12, 1991).

[2] Solenoidal Detector Collaboration, Technical Design Report, SDC-92-201, Apr. 1 1992.

[3] A. Beretvas *et al.*, SSCSIM user guide (internal note SSC-SDC-Fermilab-31).

[4] A. Para, A. Beretvas, K. Denisenko, N. Denisenko, D. Green, H. Iso, W. Wu and G. P. Yeh,"Jet Energy Resolution of the SDC Detector", Fermilab-TM-1720 (Dec. 6, 1990).

[5] W. Wu,"Updated Capabilities of SSCSIM", (internal note SSC-SDC-Fermilab-99)(1992).

[6] W. Wu, A. Beretvas, D. Green, and J. Marraffino,"Hadronic and Electromagnetic Calorimetric Segmentation", Fermilab-FN-589 (Apr. 1992).

[7] W. Wu, A. Beretvas, K. Denisenko, D. Green, J. Marraffino, and A. Para, "Monte Carlo Simulations of "Compensation" in a Calorimeter", Fermilab-FN-579 (Jan. 1992).

TABLE 1.

Stochastic and constant term coefficients

for EM and HAD compartments of the SDC calorimeter

$|\eta| < 1.5$

incident particle	Calorimeter	a	b
γ	EM	13%	1%
γ	HAD	37%	2%
hadron	EM	13%	1%
hadron	HAD	70%	2%

$|\eta| > 1.5$

incident particle	Calorimeter	a	b
γ	EM	$13\sqrt{2}\%$	1%
γ	HAD	37%	2%
hadron	EM	$13\sqrt{2}\%$	1%
hadron	HAD	70%	2%

TABLE 2.

η coverage

S_{MET} and Z^0 transverse mass resolution (measured/ISAJET)

η	Options	Cell	S_{MET} (GeV)	Transverse mass Z^0 %
5.	Off	perfect	14.5	10.9
5.	Off	normal	21.5	11.9
5.	On	normal	33.2	14.2
5.	On	perfect	41.8	16.0
3.	Off	perfect	47.8	17.0
3.	Off	normal	47.5	17.4
3.	On	normal	51.5	21.4
3.	On	perfect	55.9	22.9

TABLE 3.

Cracks S_{MET} and Z^0 transverse mass resolution (measured/ISAJET)

η	Cracks	Options	Cell	S_{MET} (GeV)	Transverse mass Z^0 %
5.	0	Off	perfect	14.5	10.9
5.	2 cm	Off	perfect	26.1	13.1
5.	4 cm	Off	perfect	39.6	16.3
5.	0	Off	normal	21.5	11.9
5.	2 cm	Off	normal	32.2	14.5
5.	4 cm	Off	normal	42.2	16.5
5.	0	On	perfect	39.6	19.0
5.	2 cm	On	perfect	41.8	20.4
5.	4 cm	On	perfect	46.0	20.2
5.	0	On	normal	30.8	14.2
5.	2 cm	On	normal	33.2	16.8
5.	4 cm	On	normal	40.8	18.4

TABLE 4.

Minimum Bias Events

S_{MET} and Z^0 transverse mass resolution (measured/ISAJET)

η	Min Bias	Options	Cell	S_{MET} (GeV)	Transverse mass Z^0 %
5.	0	Off	perfect	14.5	10.9
5.	15	Off	perfect	23.0	11.7
5.	0	On	perfect	41.8	16.0
5.	15	On	perfect	62.0	19.6

TABLE 5.

Threshold and Noise

S_{MET} and Z^0 transverse mass resolution (measured/ISAJET)

η	Threshold Noise	Options	Cell	S_{MET} (GeV)	Transverse mass Z^0 %
5.	Off	On	perfect	33.1	13.9
5.	On	On	perfect	41.8	16.0
5.	Off	On	normal	33.2	13.9
5.	On	ON	normal	33.2	14.2
3.	Off	On	perfect	53.1	19.5
3.	On	On	perfect	55.9	22.9
3.	Off	On	normal	51.8	20.9
3.	On	On	normal	51.5	21.4

TABLE 6.

photon/hadron response (e/h = 1.25)

S_{MET} and Z^0 transverse mass resolution (measured/ISAJET)

η	e/h = 1.25	Options	Cell	S_{MET} (GeV)	Transverse mass Z^0 %
5.	Off	Off	perfect	14.5	10.9
5.	On	Off	perfect	20.6	10.2
5.	Off	Off	normal	21.5	11.8
5.	On	Off	normal	23.7	11.7

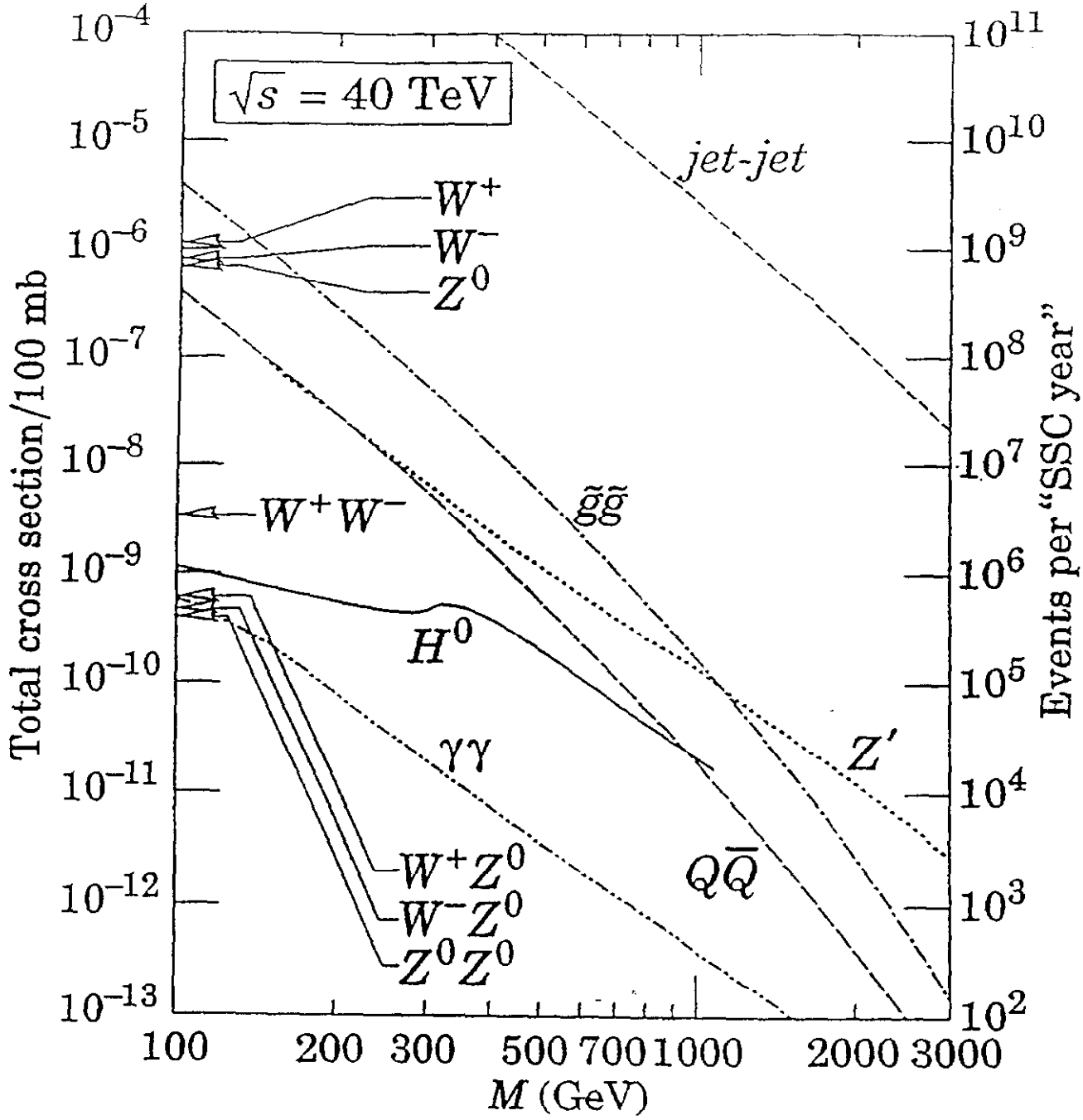

Figure 1: Examples of total cross sections at the SSC (fig 2-9 from Ref. 1).

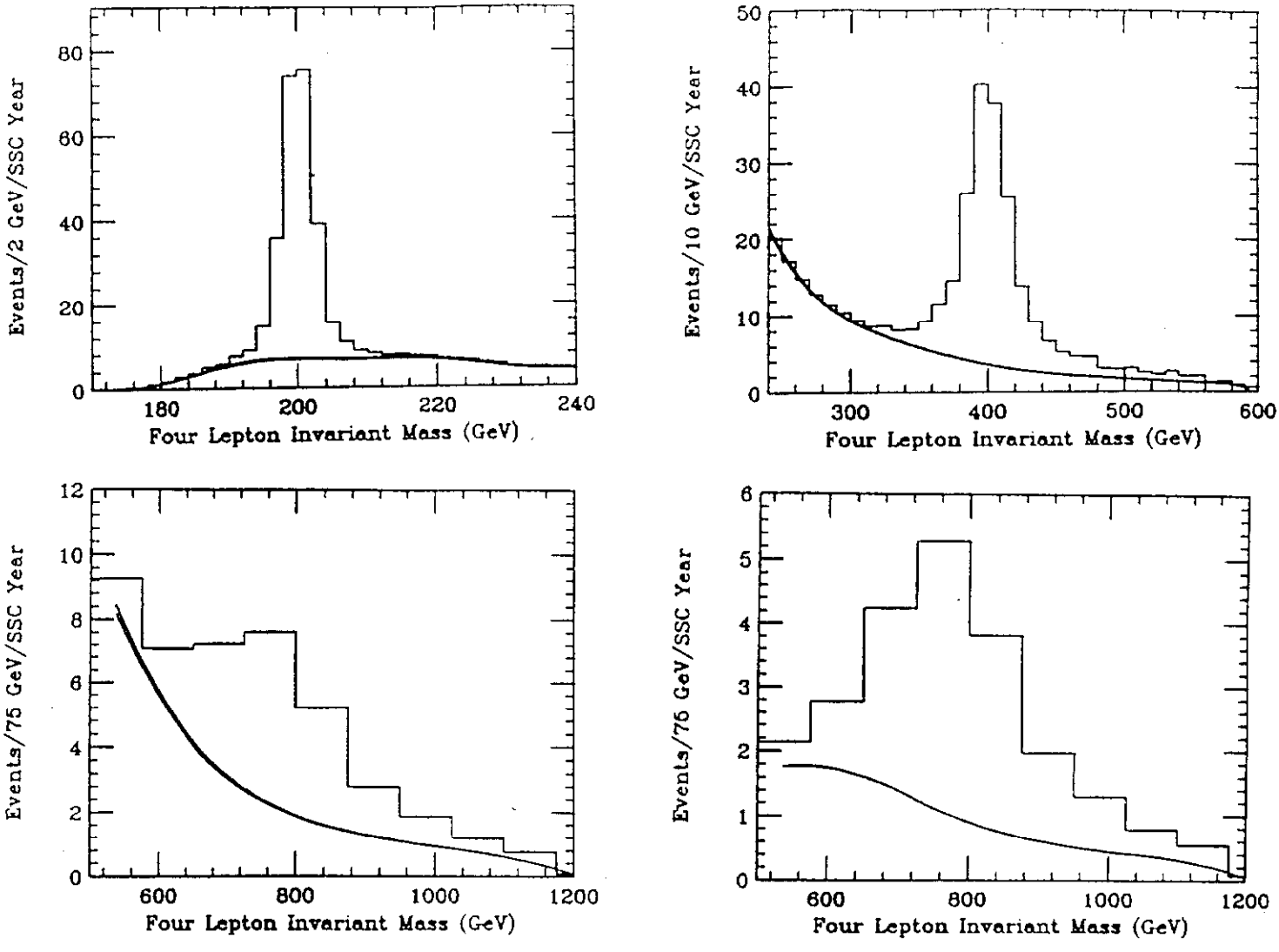

Figure 2: Four lepton invariant mass (fig 3-22, 23, 24, and 25 from Ref. 1).

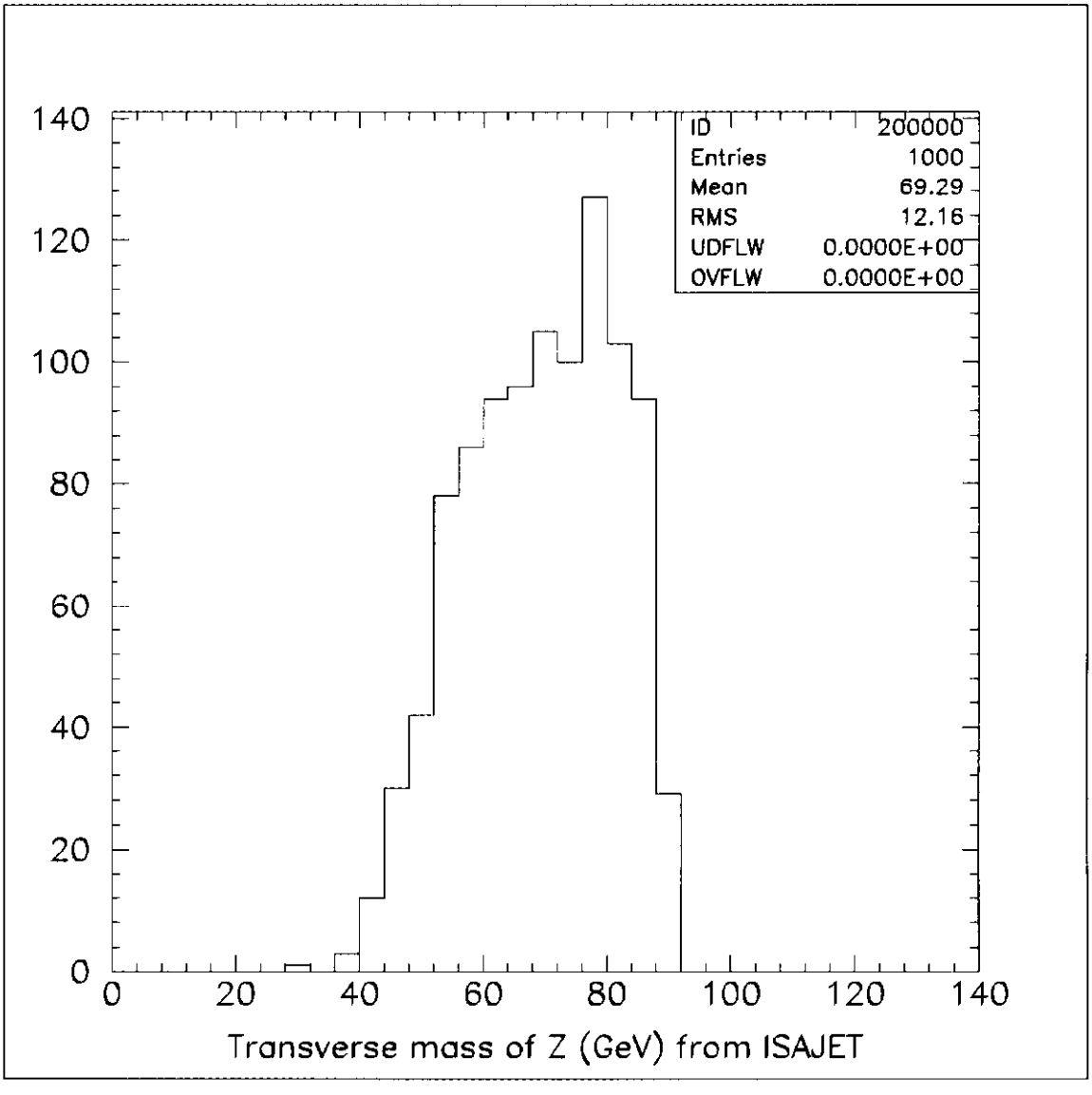

Figure 3: Transverse mass of the Z^0 (GeV/c^2) from ISAJET.

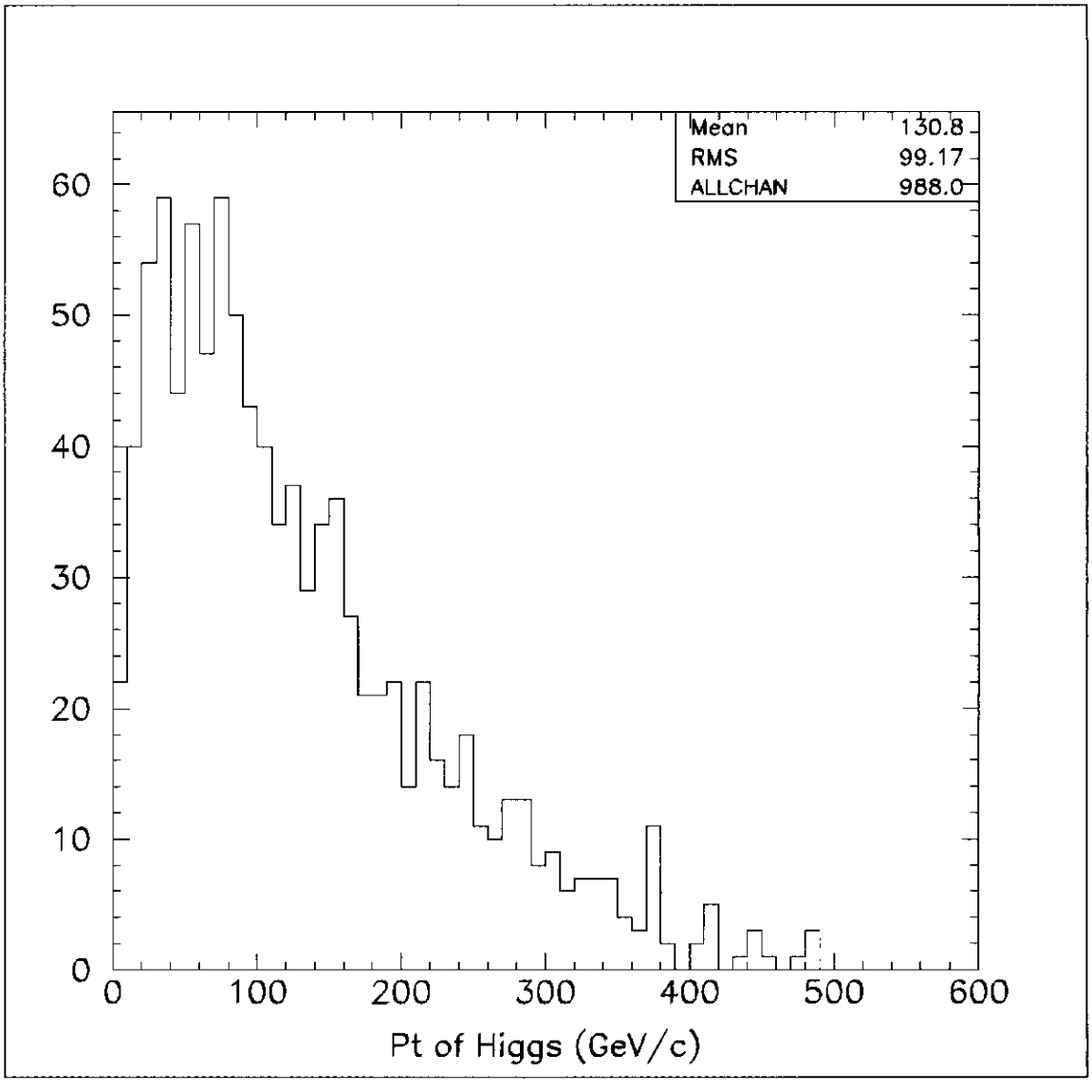

Figure 4a: The P_T (GeV/c) distribution of the Higgs.

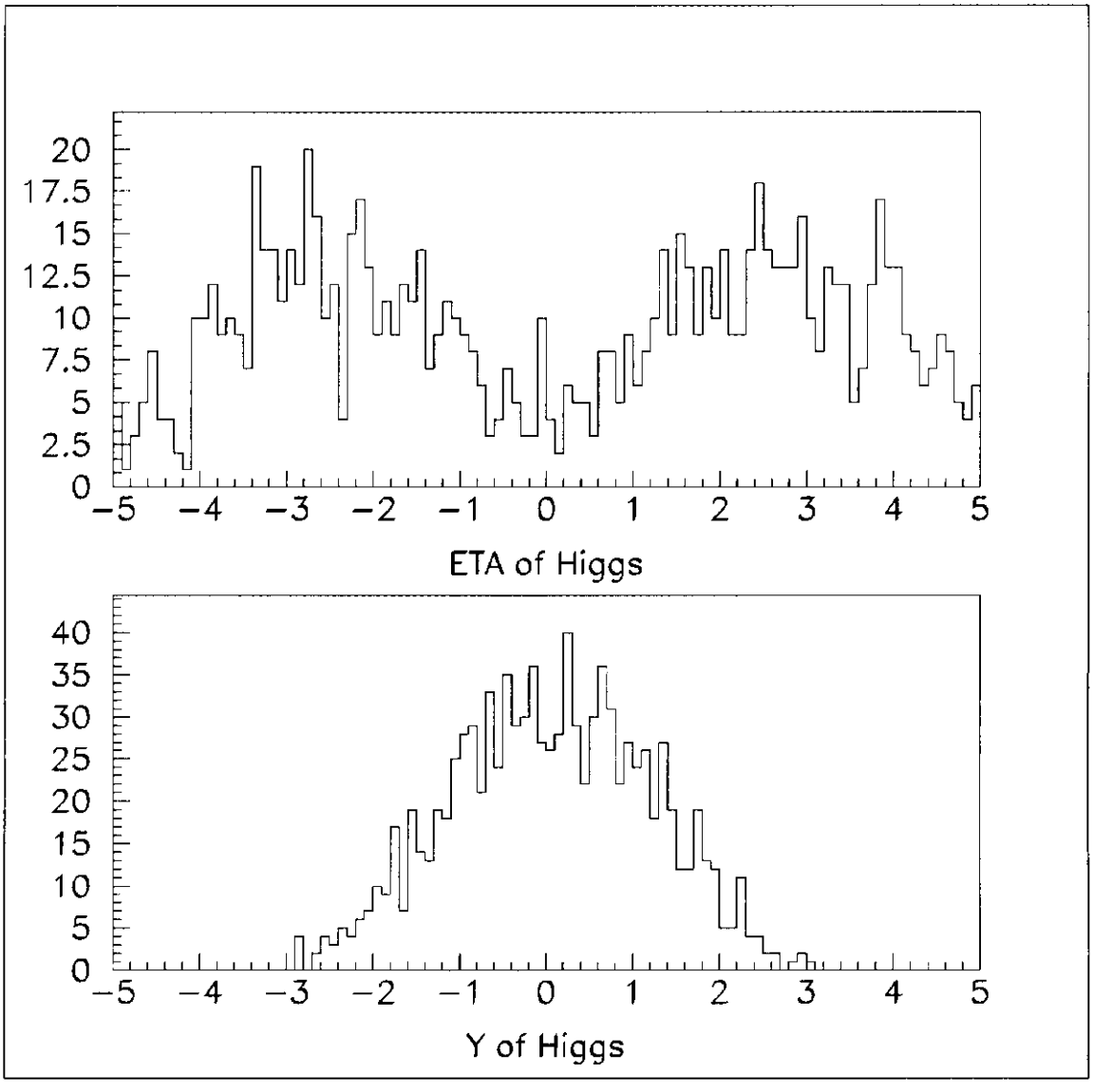

Figure 4b: The η distribution of the Higgs. (c) The rapidity (y) distribution of the Higgs.

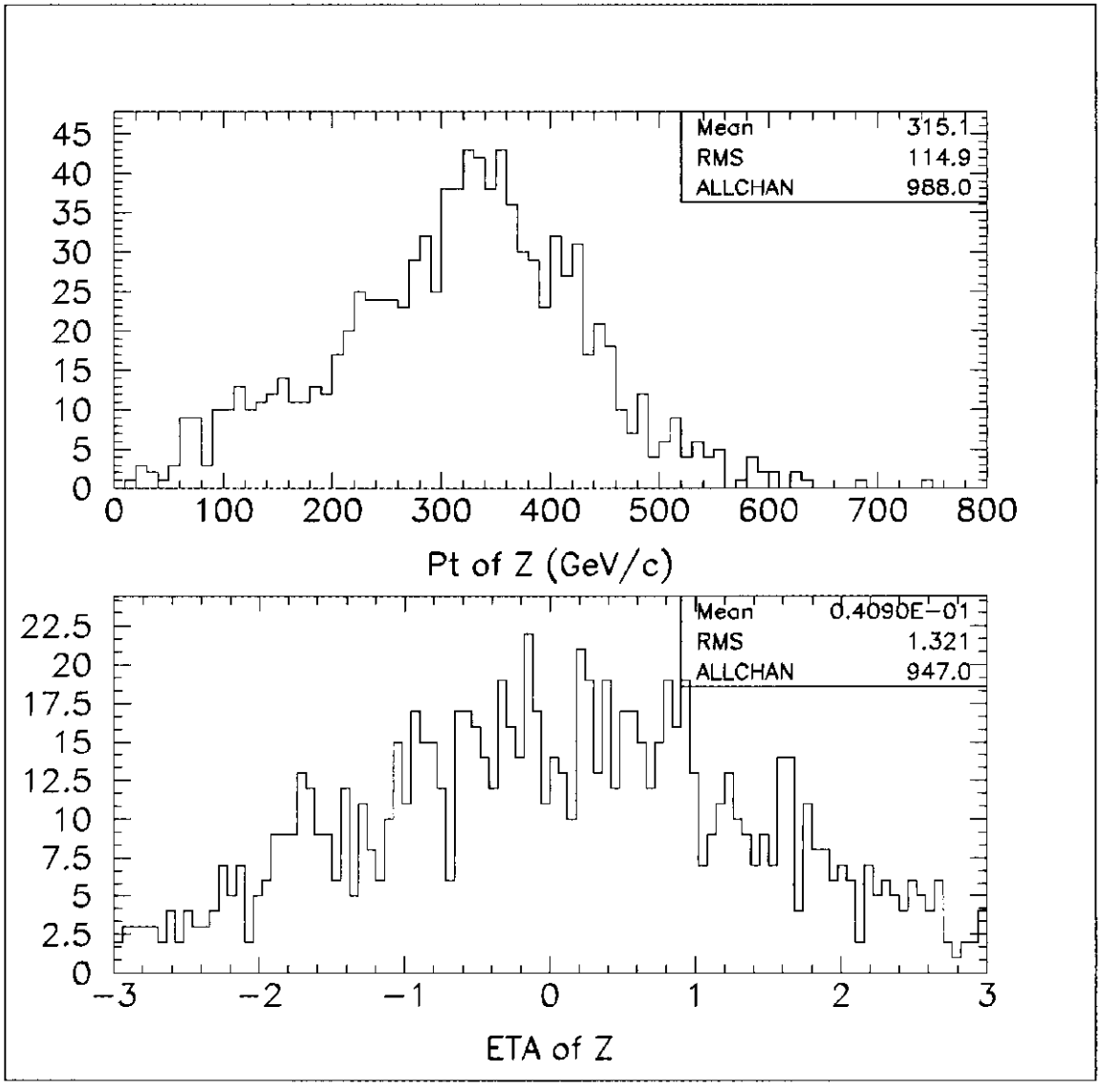

Figure 5a: The P_T (GeV/c) distribution of the Z^0. (b) The η distribution of the Z^0.

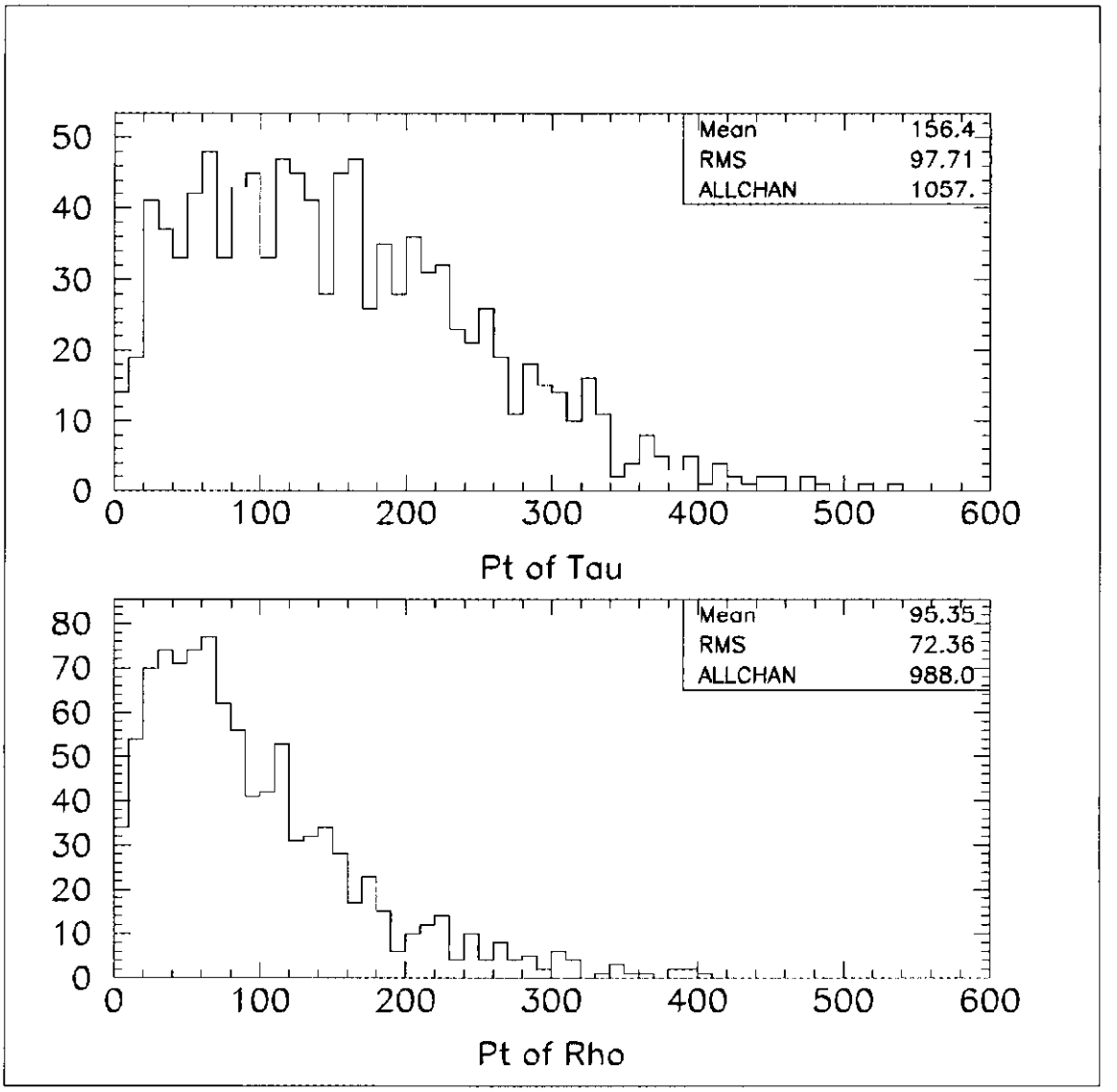

Figure 6: The P_T (GeV/c) distribution of the (a) τ, and (b) ρ.

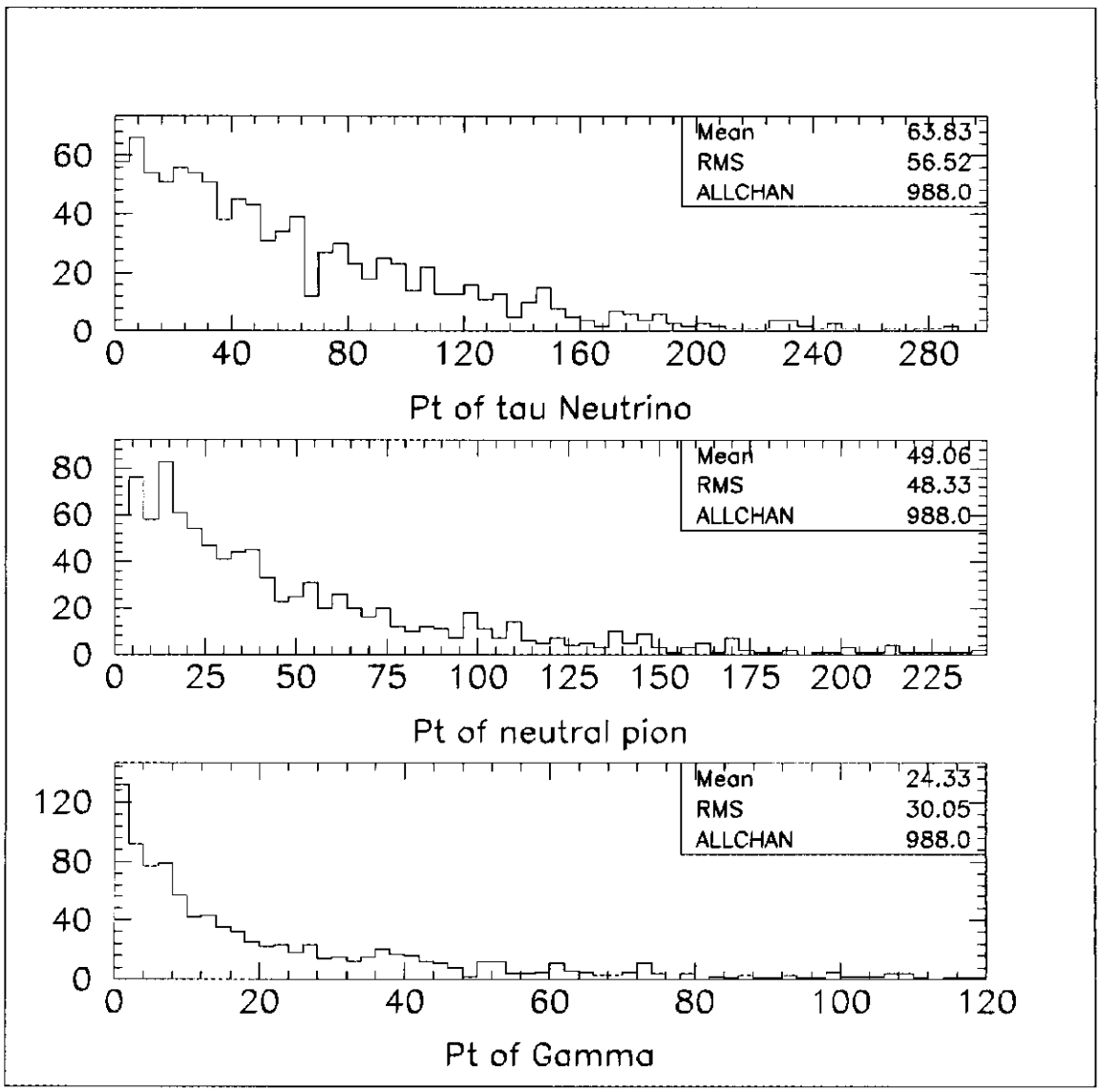

Figure 6: The P_T (GeV/c) distribution of the (c) ν, (d) π, and (e) γ.

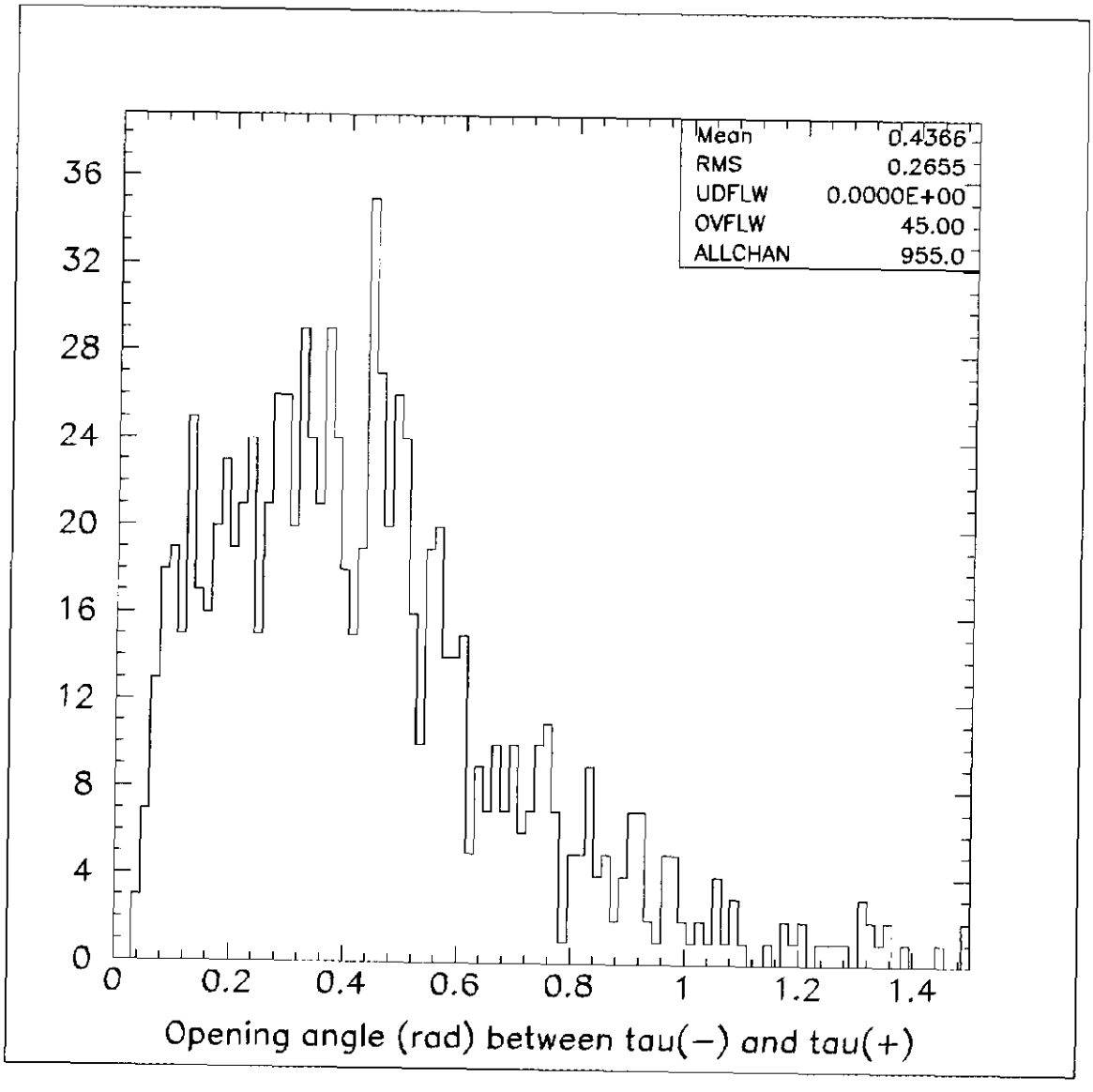

Figure 7: The opening angle between the τ^+ and τ^-.

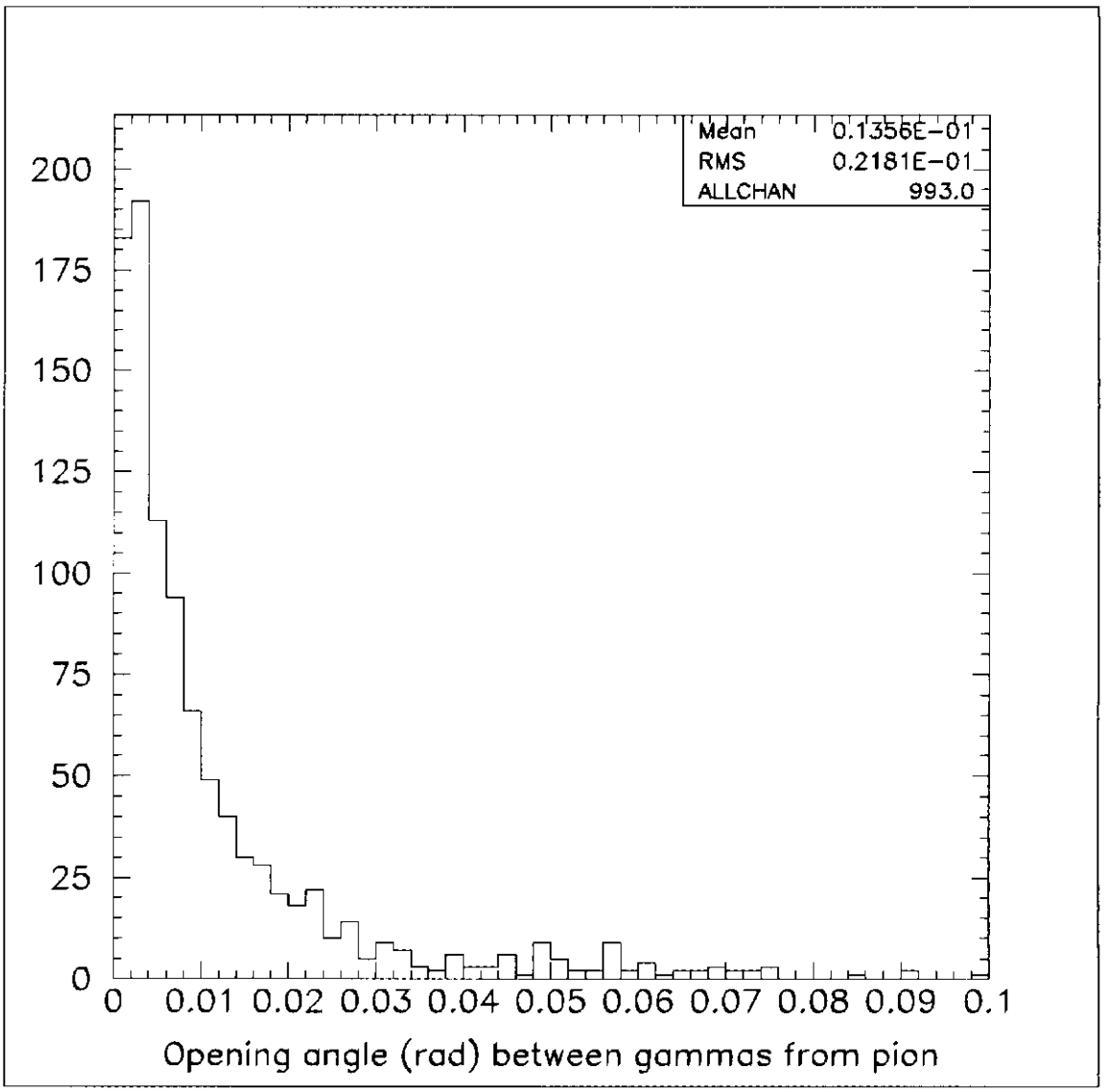

Figure 8a: The opening angle between the two γ's.

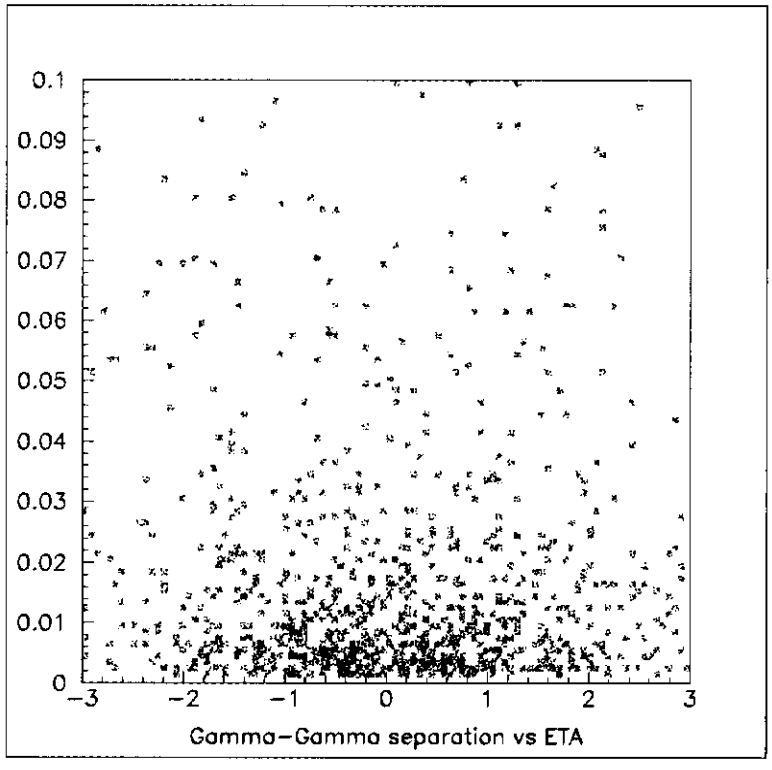

Figure 8b: A scatterplot of the opening angle between the two γ's versus η.

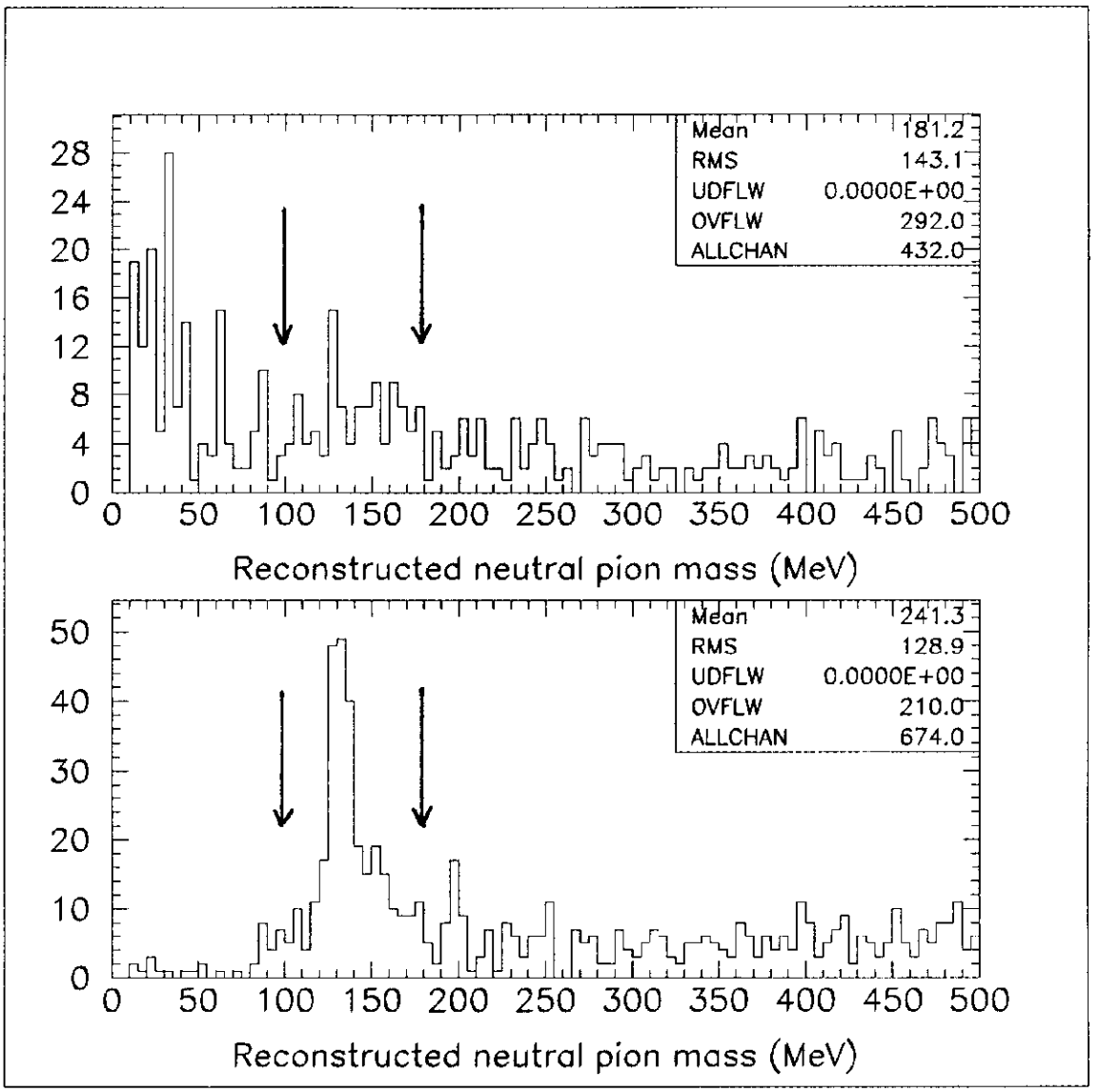

Figure 9: The mass of the reconstructed π^0 (GeV/c^2) (a) for EM calorimeter cell size of $\Delta\eta = \Delta\phi = 0.05$ (b) cell size $\Delta\eta = \Delta\phi = 0.00625$. Cuts are indicated by the arrows for both plots.

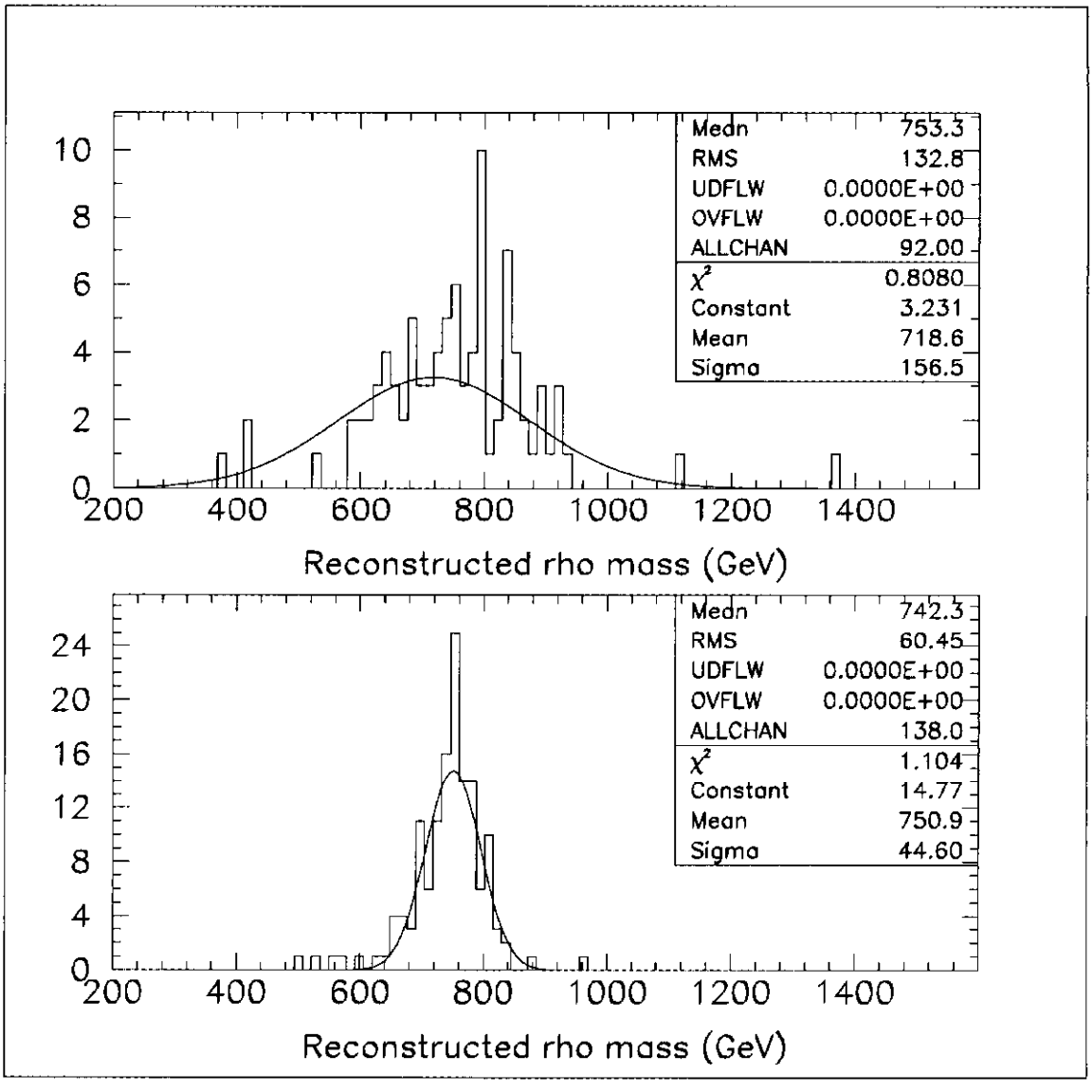

Figure 10a: The mass of the reconstructed ρ (GeV/c^2) (a) for EM calorimeter cell size of $\Delta\eta = \Delta\phi = 0.05$ (b) cell size $\Delta\eta = \Delta\phi = 0.00625$.

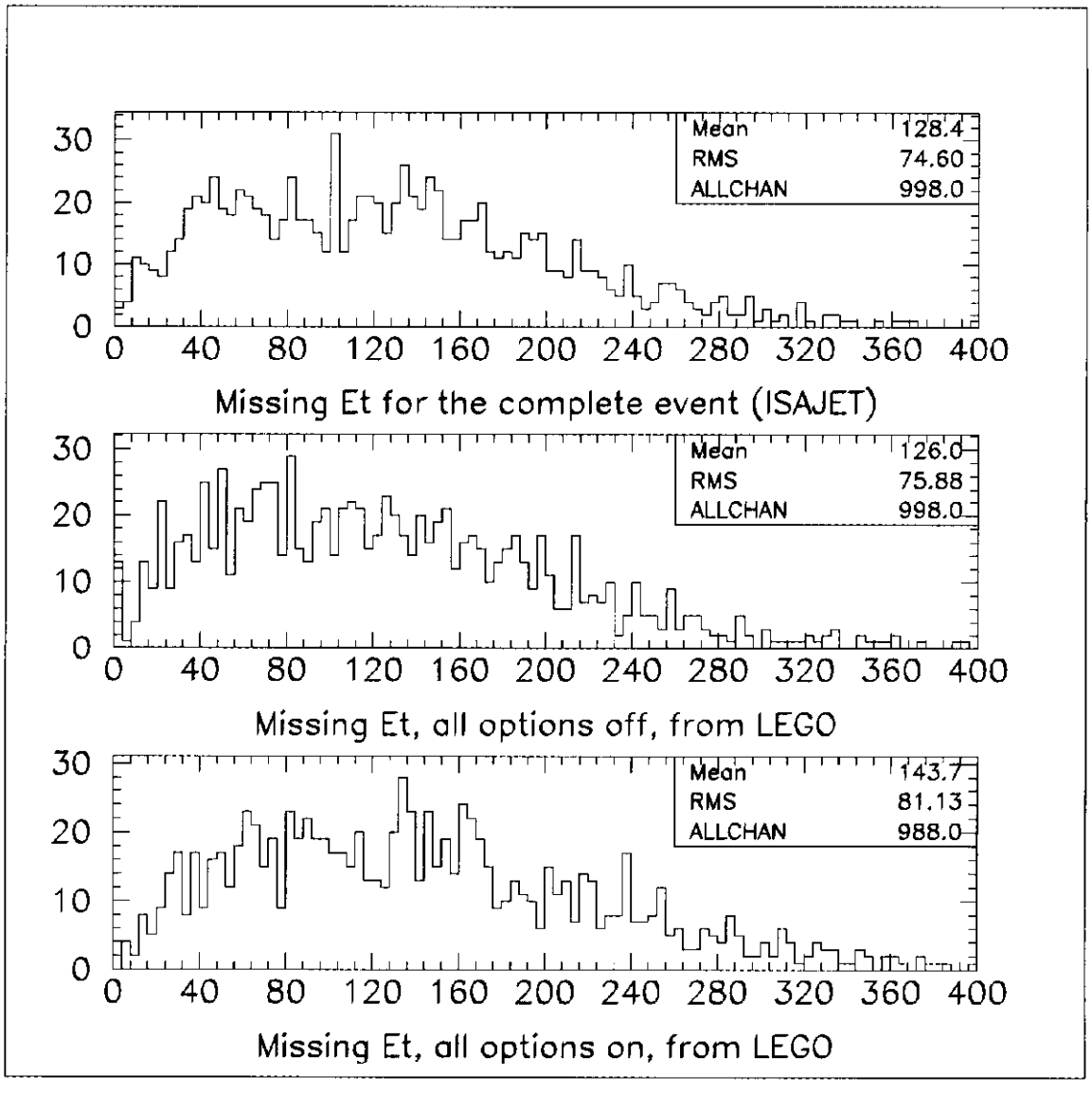

Figure 11: Missing transverse energy (GeV/c^2) (a) for the complete event (ISAJET) (b) for an ideal detector that extends out to $\eta = 5$.(all option off) (c) same as (b) but with all options on.

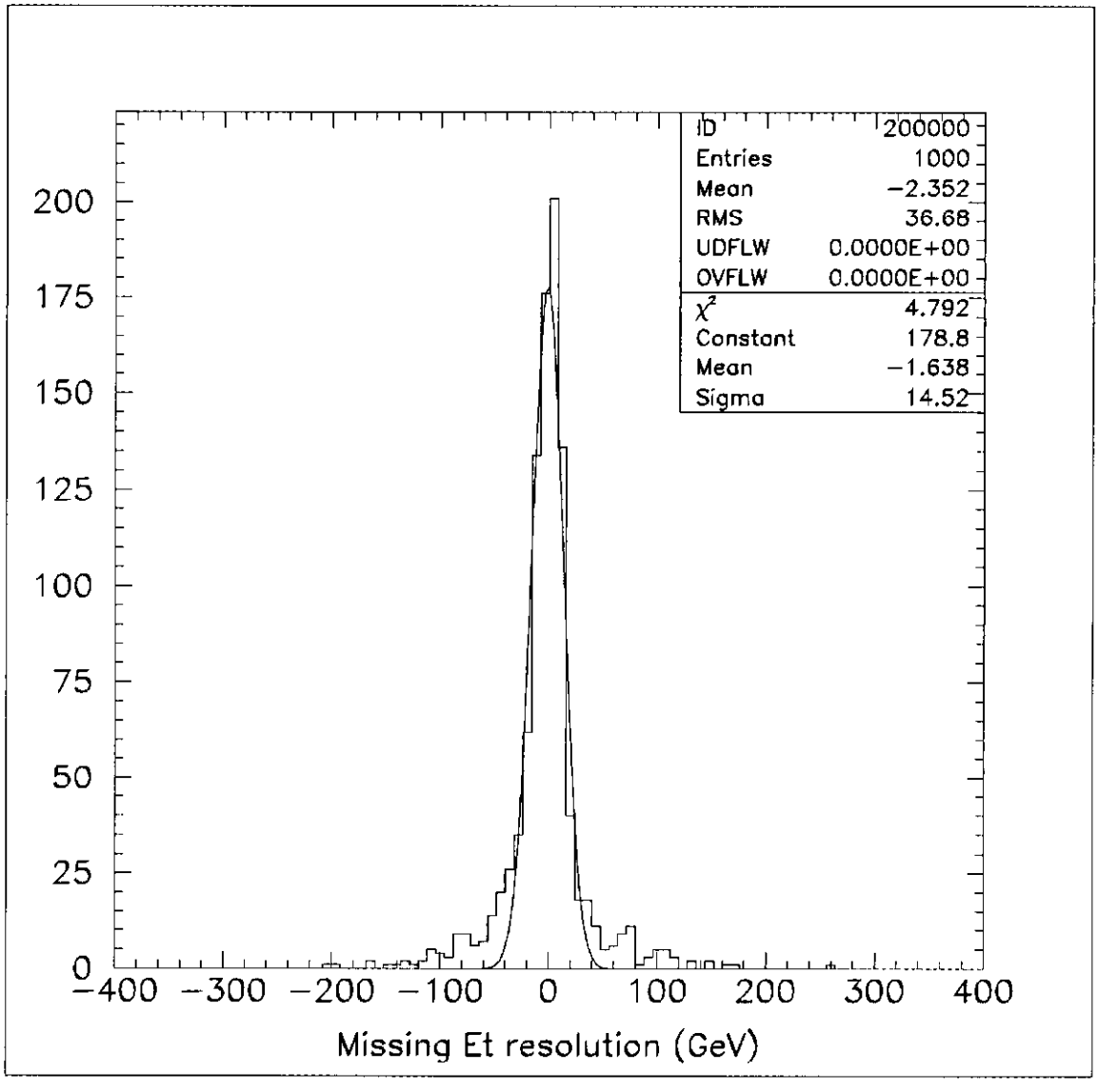

Figure 12a: The distribution S_{xy} (GeV/c^2) is plotted (the difference between the measured missing E_T and ISAJET) along with a Gaussian fit with a mean of 14.5 $(GeV/c^2) = S_{MET}$.

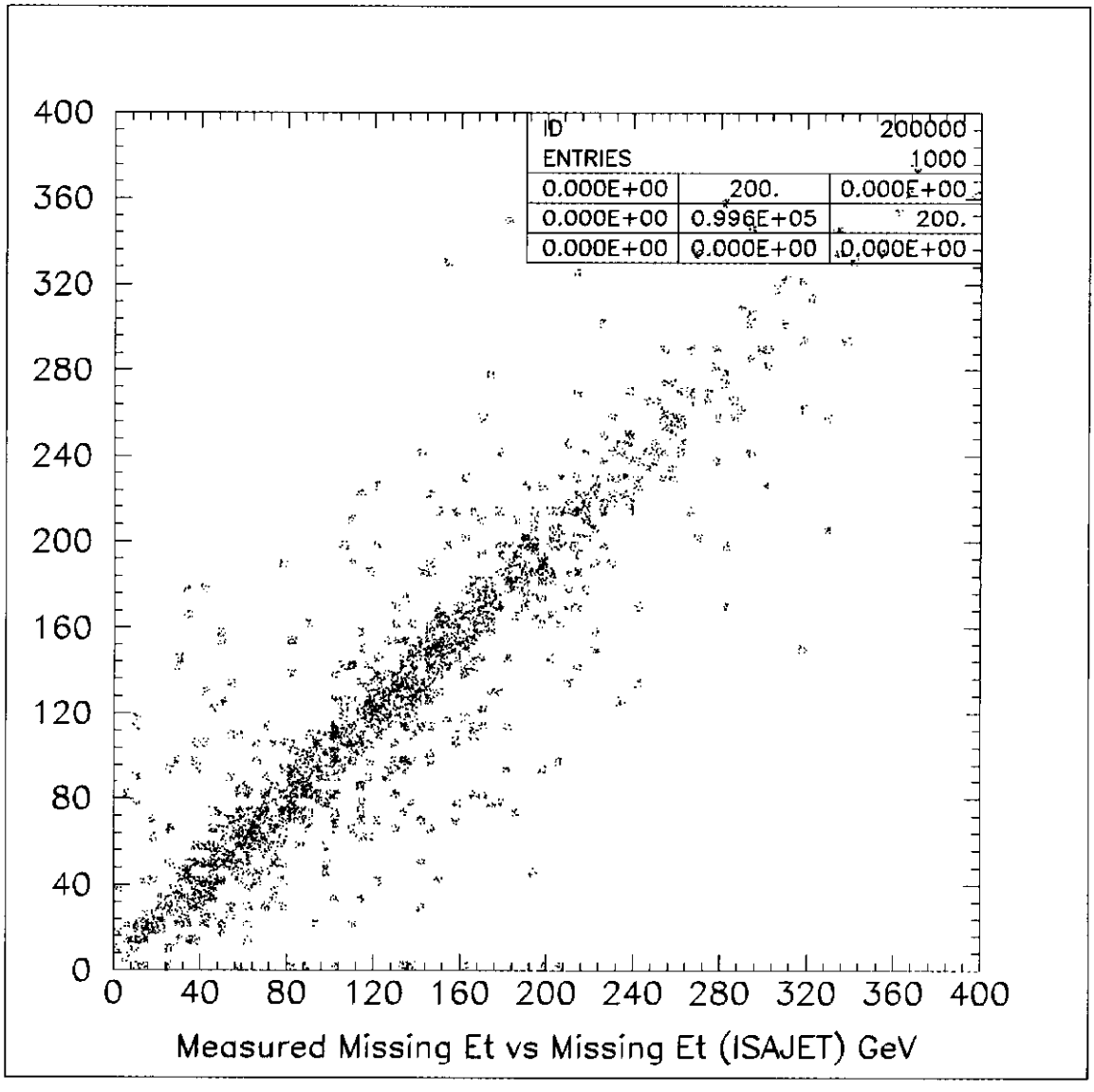

Figure 12b: A scatter plot of measured missing E_T (GeV/c^2) versus missing E_T obtained from ISAJET.

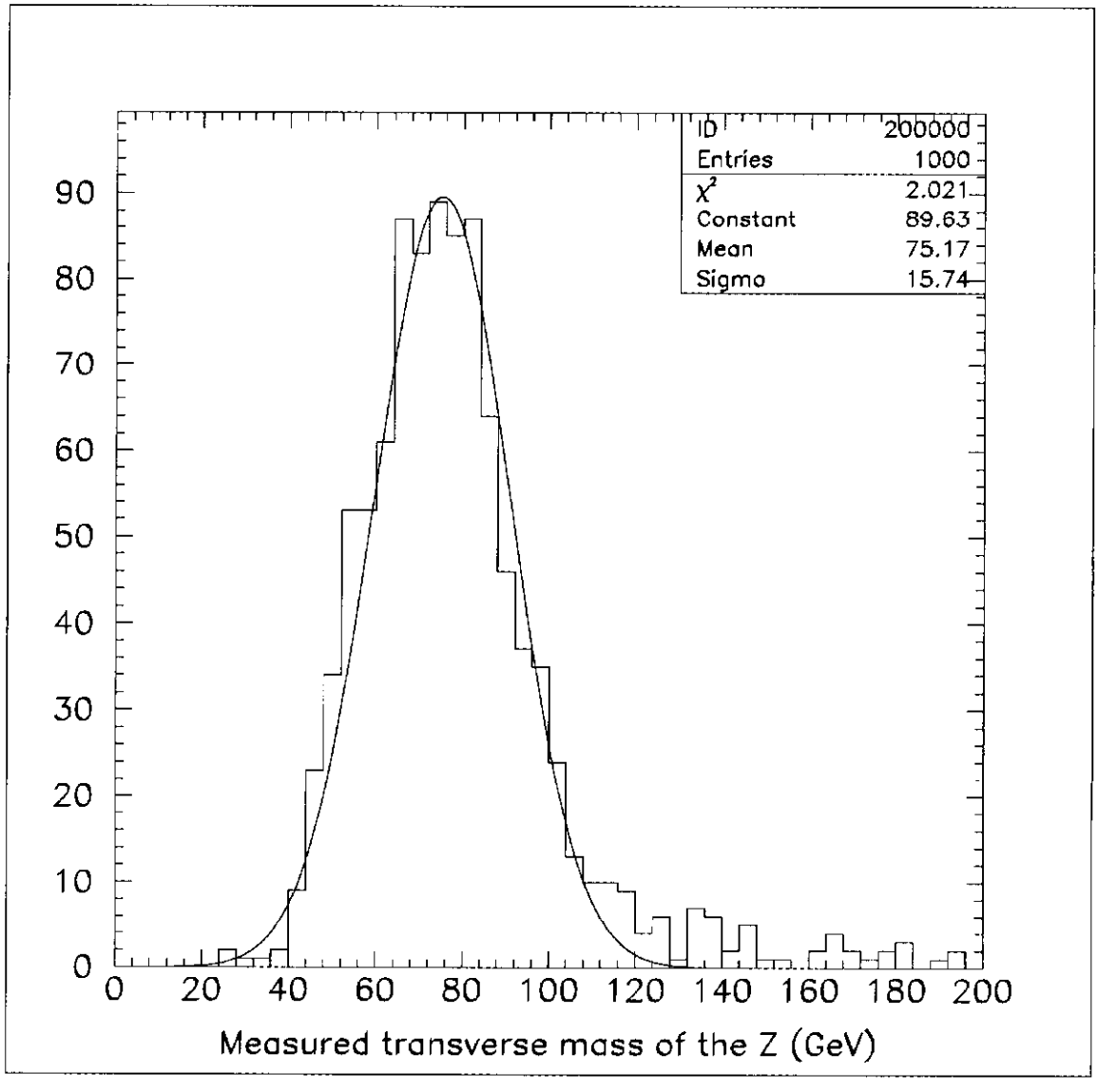

Figure 13: Transverse mass of the Z^0 (GeV/c^2) for a detector that extends out to $\eta = 5.0$ that has "perfect" cell size and has all options turned off.

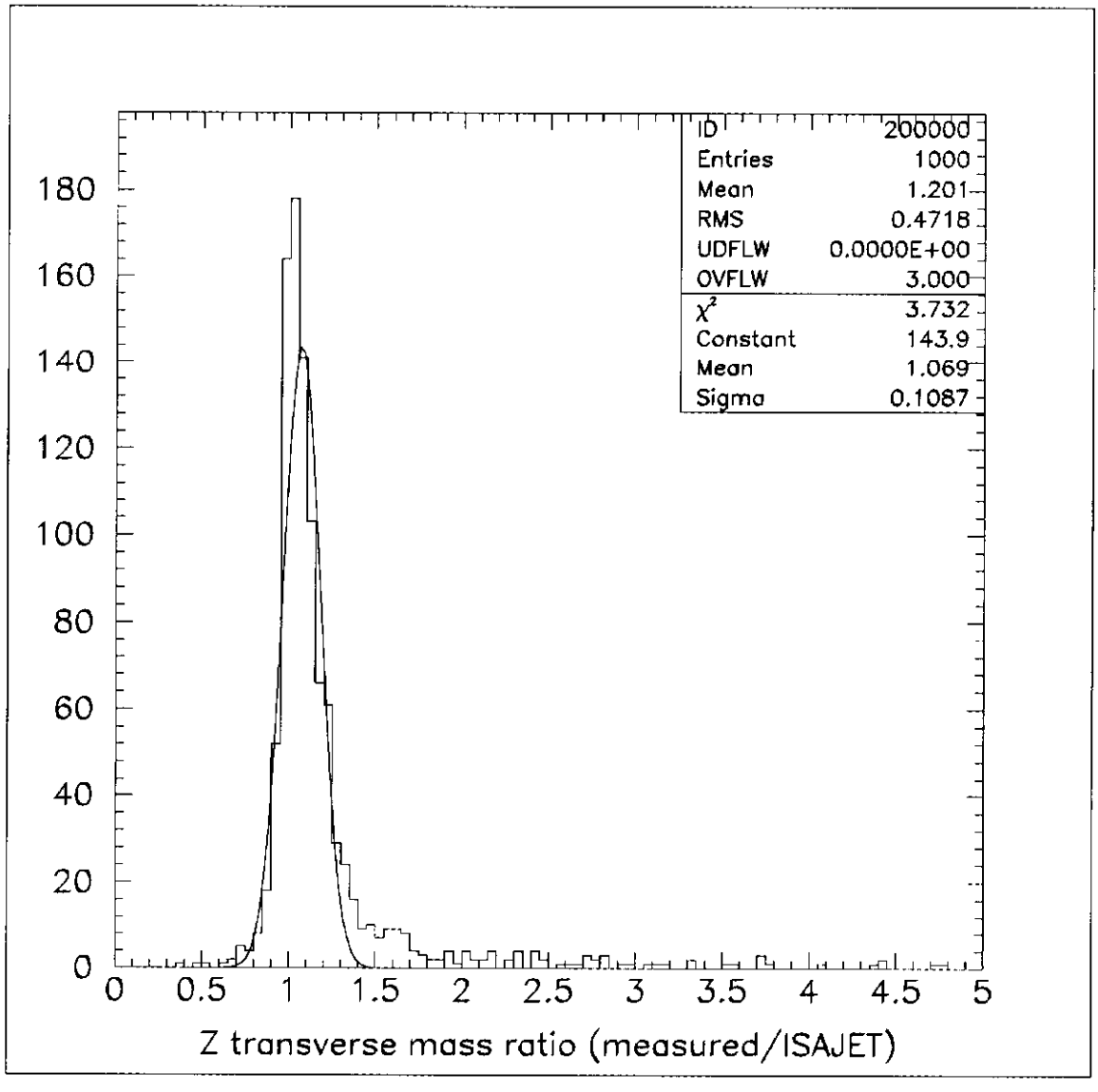

Figure 14: Ratio (measured/ISAJET) of transverse mass of the Z^0 for a detector that extends out to $\eta = 5.0$ that has "perfect" cell size and has all options turned off.

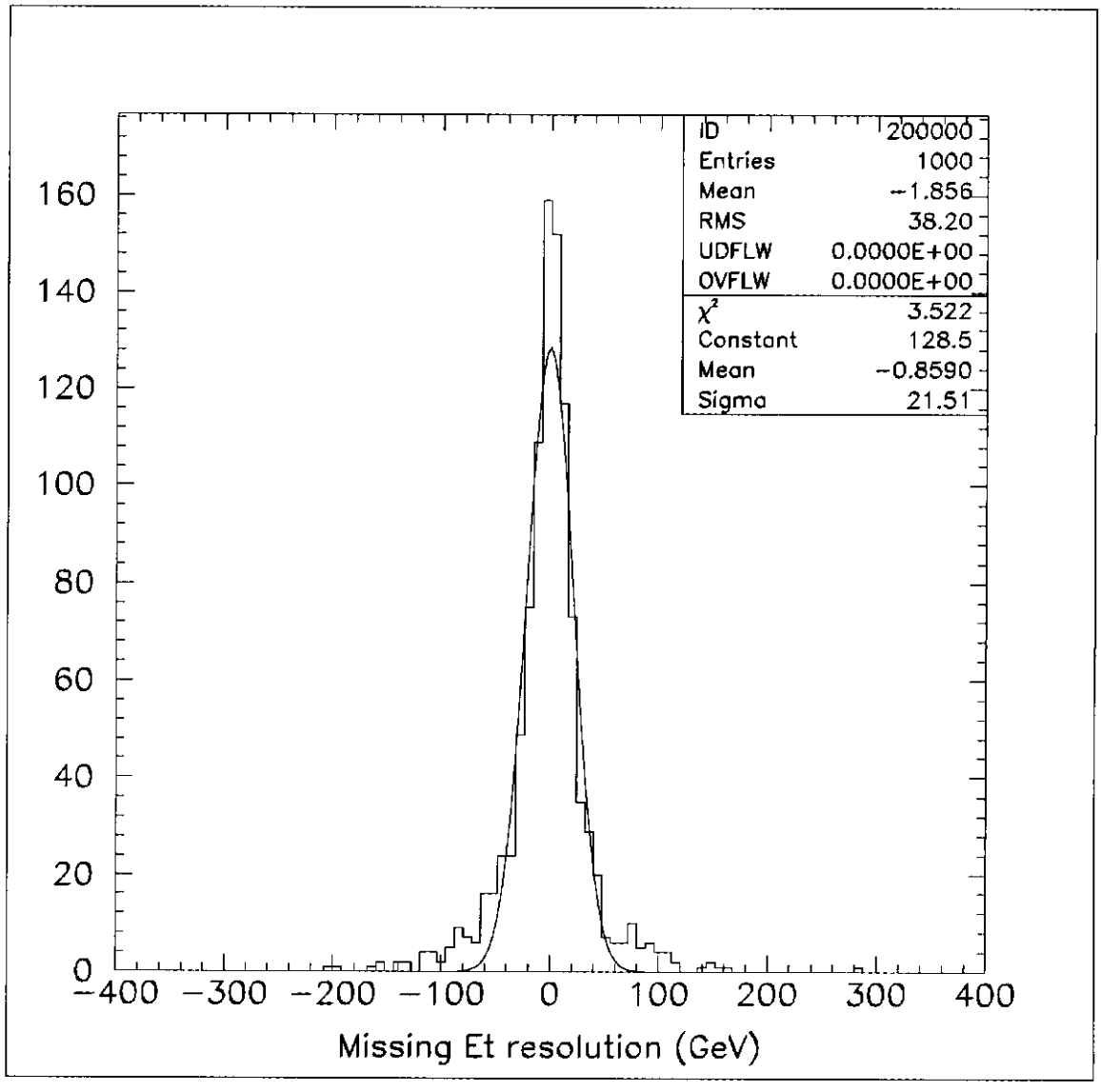

Figure 15a: Deviation of missing energy from that given by ISAJET.

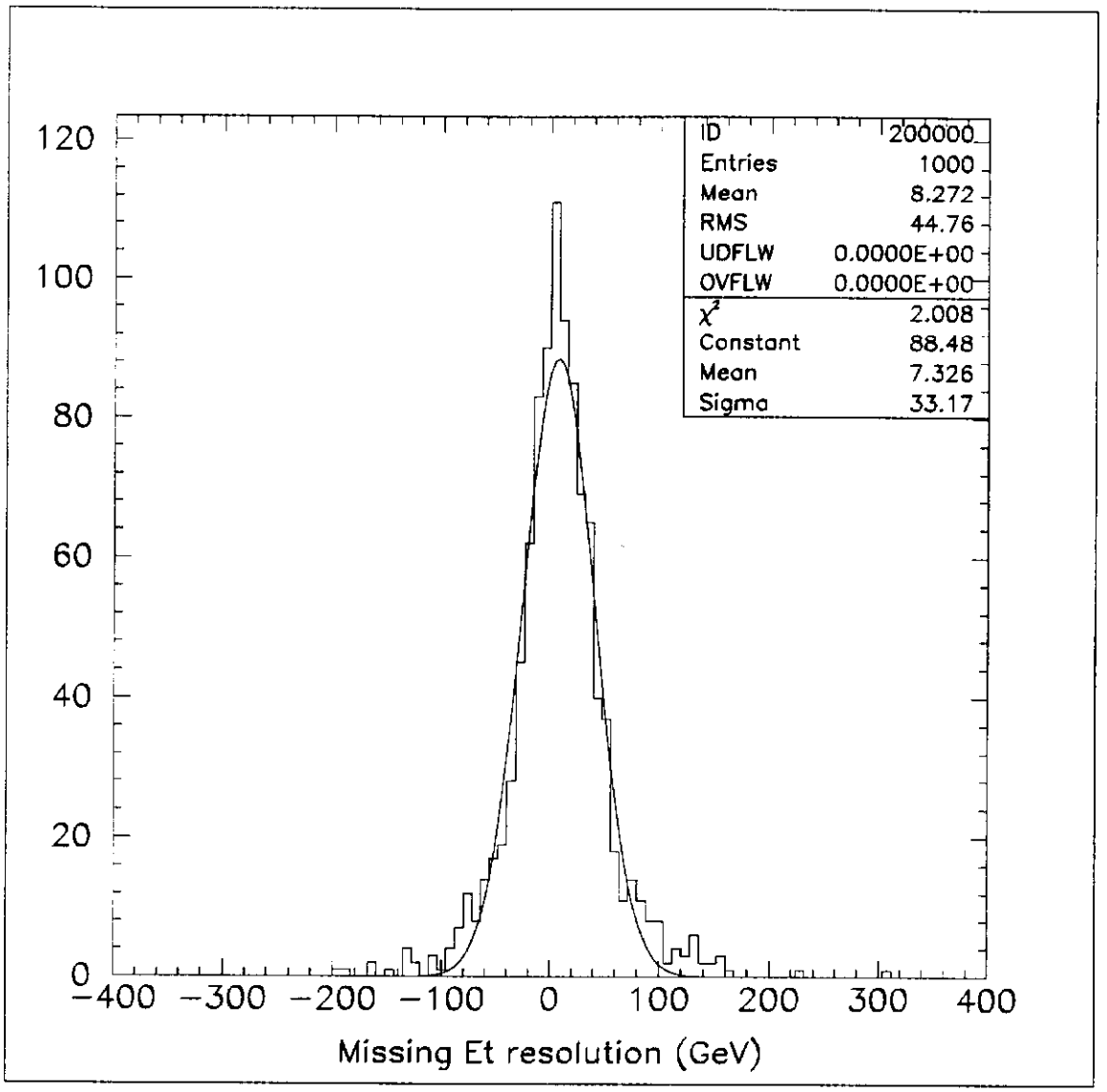

Figure 15b: Deviation of missing energy from that given by ISAJET same as above but with all options turned on.

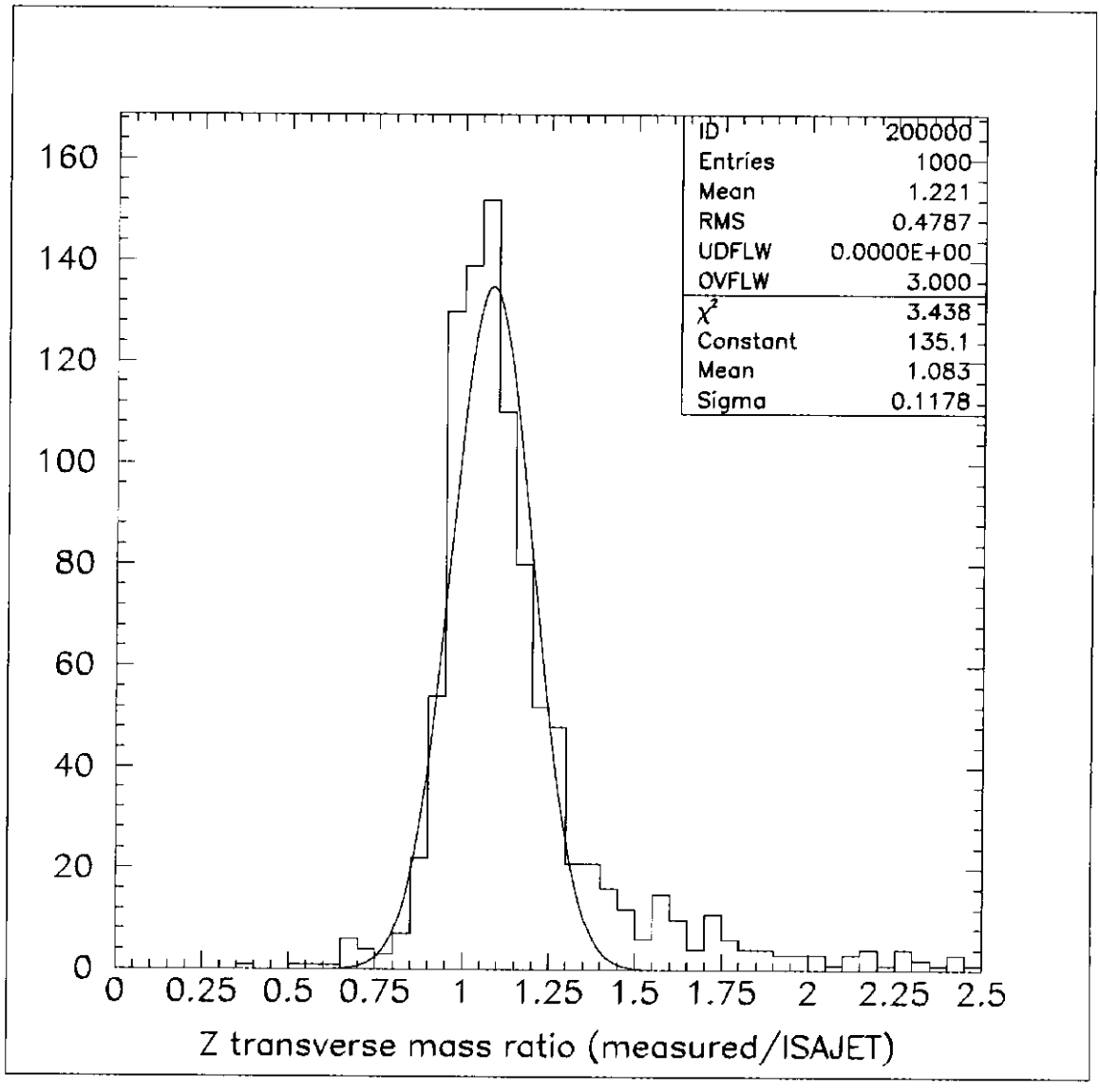

Figure 16a: Ratio (measured/ISAJET) of transverse mass of the Z^0 for a detector that extends out to $\eta = 5.0$ that has "normal" cell size and has all options turned off.

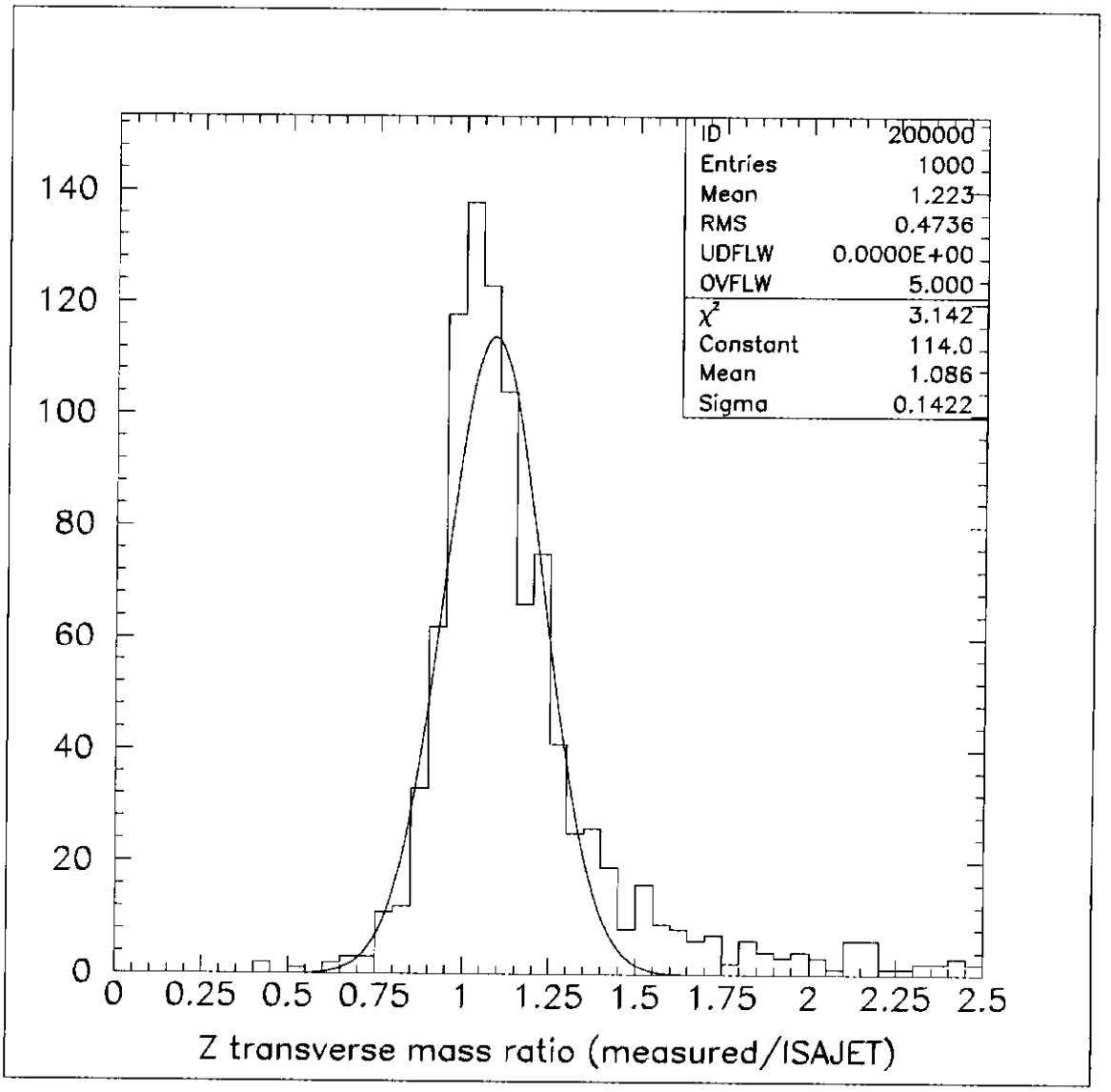

Figure 16b: Ratio (measured/ISAJET) of transverse mass of the Z^0 for a detector that extends out to $\eta = 5.0$ that has "normal" cell size and has all options turned on.